47th AIAA Aerospace Sciences Meeting Including The New Horizons Forum and Aerospace Exposition
5 - 8 January 2009, Orlando, Florida

AIAA 2009-874

Experiment-Based Optimization of Flapping Wing Kinematics

Scott L. Thomson[1], Christopher A. Mattson[2], Mark B. Colton[3],
Stephen P. Harston[4], Daniel C. Carlson[5], Mark Cutler[6]
Department of Mechanical Engineering, 435 CTB, Brigham Young University, Provo, UT, 84663

Optimization of flapping wing trajectory was explored using an experimental apparatus. A scaled-up hawkmoth (*Manduca sexta*) wing was fabricated and mounted to a three-degree of freedom flapping mechanism. The vertical force generated during flapping was measured using a load cell and the wing path was optimized to maximize the average vertical force. The mechanism design, control, and instrumentation, and the optimization approach are explained. The optimization results, including wing trajectories, are presented and further research topics are discussed.

Nomenclature

$A_{i,j}$	=	amplitudes for driving functions (°)
F_z	=	vertical force (arbitrary units)
t_s	=	sampling duration (s)
α	=	wing feathering angle (°)
α_d	=	desired wing feathering angle (°)
φ	=	wing flapping angle (°)
φ_d	=	desired wing flapping angle (°)
θ	=	wing elevation angle (°)
θ_d	=	desired wing elevation angle (°)
ω	=	driving function fundamental frequency (rad/s)

I. Introduction

Micro air vehicles (MAVs) – vehicles with a maximum dimension of no more than 15 cm[1] – offer attractive solutions for various applications, such as surveillance, reconnaissance, and search and rescue operations. Along with reduced size is a change in aerodynamic flight regime characterized by a relatively low Reynolds number. In this regime, flapping flight introduces several aerodynamic advantages, as evidenced by the ubiquitous use of flapping flight by various animals (for example, about 75% of the approximately 13,000 species of warm-blooded vertebrates fly[2]). Miniaturization of man-made flapping wing flying vehicles is desirable because of advantages such as reduced detectability (due to small size and possible reduced noise), the ability to hover and/or perch-and-stare, and potentially enhanced ability to navigate relatively small, confined spaces (such as a building).

Many aspects of flapping flight aerodynamics, however, are yet to be fully understood. Such aspects include unsteady aerodynamic lift-enhancing phenomena, identification of separation and reattachment points, and laminar-to-turbulent transition. In nature, deformable and/or adjustable wings and wing kinematics add to this complexity, in addition to effects such as the wide variability in wing size, shape, and kinematics found between various species. An increased understanding of such phenomena has the potential to significantly improve MAV capabilities.

[1] Assistant Professor, Mechanical Engineering, AIAA Member.
[2] Assistant Professor, Mechanical Engineering, AIAA Member.
[3] Assistant Professor, Mechanical Engineering.
[4] Research Assistant, Mechanical Engineering, AIAA Student Member.
[5] Research Assistant, Mechanical Engineering.
[6] Research Assistant, Mechanical Engineering.

A significant amount of research, both experimental and computational, has focused on flapping flight aerodynamics. A few recent experiment-based studies are mentioned here which have included a study of optimal flapping motion. Dickinson et al.[3] built and used a scaled-up robotic mechanism to simulate and explore the wing motion of the fruit fly, *Drosophila melanogaster*. Various mechanisms that contributed to enhanced aerodynamic performance were studied, including delayed stall, rotational circulation, and wake capture. Other flapping mechanisms have been constructed; for example, Conn et al.[4] described a crank-rocker flapping mechanism for the purpose of optimizing wing kinematics, and Bandyopadhyay et al.[5] used a robotic penguin pectoral wing to determine optimal fin kinematics for efficiency during forward motion and during hover.

The goal of our present research is to first develop and then use a flapping wing mechanism to seek for and investigate optimal paths for various wing configurations (including compliant wings) and optimization objectives. Our motivation includes the following. First, approaches based on computational fluid dynamics (CFD) simulations are very time consuming, especially when considering the number of simulations needed to explore the relatively large design space. Moreover, CFD methodologies which incorporate fully-coupled deformable wings are still being developed. Second, fast and efficient low-order analytical methods, such as those which have been used for traditional fixed-wing aerodynamic analysis, are not yet available for compliant, flapping wings with arbitrary kinematics. Experiment-based optimization has the potential to mitigate these difficulties in that it is significantly faster than CFD, allows for wing compliance, and does not contain limitations regarding modeling relevant flow physics. Third, we observe that many flying animals utilize various wing trajectories that are presumably optimal for a given size, shape, and flight mode (e.g., hovering vs. takeoff or landing). However, these wing trajectories may not necessarily be optimal for MAVs with manmade wing actuation and design objectives. As a first step towards our goal, we have designed and constructed a flapping wing mechanism with three degrees of freedom corresponding to three flapping angles. Results of the aerodynamic forces, including optimization of the path of a given wing for maximum average vertical force, are presented.

II. Methods

A. Overview

Our current research approach is to construct a flapping wing (including instrumentation and control hardware) and optimize the wing trajectory for maximum average vertical force. The approach of experimental optimization was chosen to avoid the cost of computational methods, the uncertainty in complex flow physics prediction (unsteady separation, transition to turbulence, turbulence itself), and difficulty associated with moving-grids when using traditional body-fitted methods. The long-term goal is to use this mechanism design to explore the aerodynamic phenomena associated with optimal wing kinematics.

B. Wing Design

The wing (shown in Fig. 1) is roughly based on that of the hawkmoth, *Manduca sexta* (the subject of several computational[6] and experimental[7] studies). We note, however, that the shape of the wing in the present study is somewhat arbitrary, and that the chosen scaling criteria (based on Reynolds and Strouhal numbers) were not based on those of the hawkmoth. The wing was scaled up to approximately 11 cm and is driven at a frequency of 0.5 Hz in transformer oil (density = 874 kg/m^3, dynamic viscosity = 0.013 Pa·s). To minimize inertial effects of the wing itself, the wing was fabricated of thin balsa wood. The wing was mounted on a flapping mechanism (described below).

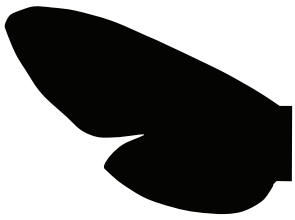

Figure 1. Wing outline.

C. Flapping Mechanism

A three degree-of-freedom (DOF) robotic mechanism was constructed to enable basic rigid body flapping motion, with capabilities roughly similar to the mechanism developed by Dickinson et al.[3] The mechanism is shown in Fig. 2. The three motion DOFs are achieved by rotating the vertical shaft through the elevation angle (θ) about the ground-fixed vertical axis, rotating the inner gimbal through the flapping angle (φ) about the shaft-fixed horizontal gimbal axis, and rotating the wing through the feathering angle (α) about the inner gimbal-fixed wing axis. All three axes of rotation intersect at a single point (called "the shoulder") in the center of the inner gimbal. Three Maxon brushed DC motors, driven by Advanced Motion Controls PWM servo amplifiers, actuate the wing motions. The mechanism was designed to allow for interchangeable wings so that a variety of wings (including rigid and compliant wings) can be tested.

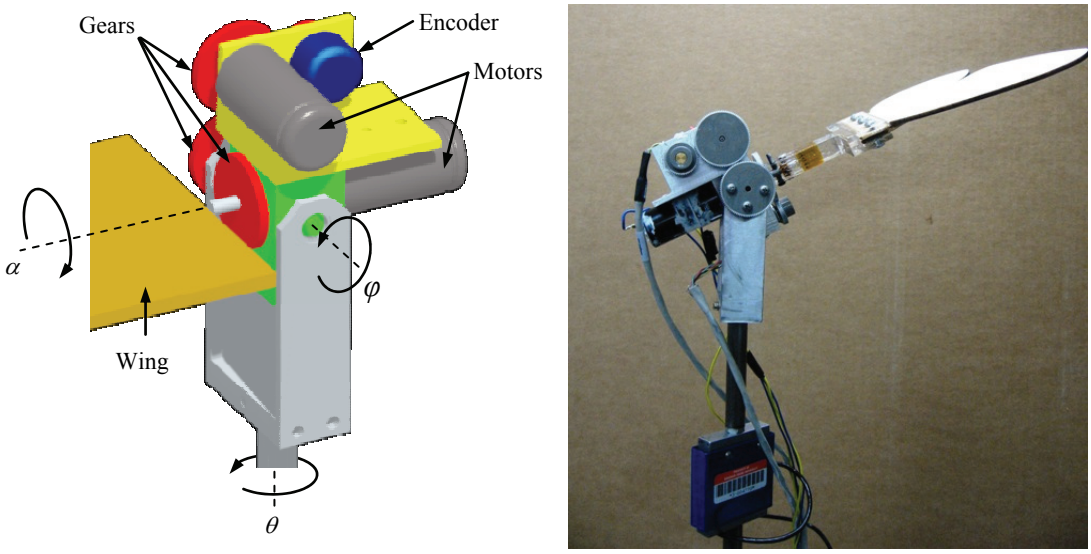

Figure 2. Flapping mechanism CAD model (left) and photo (right).

D. Instrumentation

The object of the instrumentation is to measure the flapping angles (θ, φ, α) and the average vertical flapping force ($\overline{F_z}$). The flapping angle trajectories are measured using three US Digital incremental encoders, one mounted to each shaft. A load cell capable of measuring tensile and compressive forces was mounted in the vertical shaft to measure $F_z(t)$ as the wing executes each pre-defined motion trajectory. At the beginning of each experimental run, the force bias is subtracted in software to minimize the effects of temperature drift.

E. Control

A three-channel controller was developed to cause the flapping mechanism to track the desired angle trajectories $\theta_d(t)$, $\varphi_d(t)$, and $\alpha_d(t)$, as shown in Fig. 3. The controller was developed in LabVIEW and implemented on a National Instruments (NI) CompactRIO Real-Time Controller (cRIO-9002) with NI 9205 and NI cRIO-9263 analog interface modules. The control loop was run at a rate of 1 kHz and the PID control gains were tuned experimentally to ensure stability and satisfactory trajectory tracking. Position feedback was provided by the incremental encoders described previously. Gravity compensation on the flapping angle (φ) DOF was implemented to maintain accurate tracking in the presence of the gravity disturbance.

In each iteration of the experiment, the control code reads in the desired flapping trajectories $\theta_d(t)$, $\varphi_d(t)$, and $\alpha_d(t)$, which are generated by the optimization code running in MATLAB, executes the motion trajectories, records the angle and force data from the encoders and load cell, and stores the data for use by the MATLAB optimization code. MATLAB then uses these data to generate a new set of desired trajectories, which are again executed by the control software.

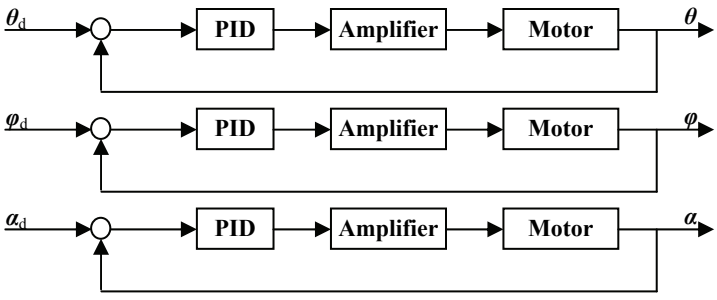

Figure 3. Three-channel control with axis decoupling. Gravity compensation not shown.

F. Kinematics

The desired flapping trajectories were defined using the first four terms of a Fourier series expansion for each DOF, in a manner similar to that employed by Aono et al.[8] (only using fewer terms):

$$\begin{aligned}\theta_d(t) &= A_{11} + A_{12}\sin\omega t + A_{13}\cos\omega t + A_{14}\sin 0.5\omega t \\ \varphi_d(t) &= A_{21} + A_{22}\sin\omega t + A_{23}\cos\omega t + A_{24}\sin 0.5\omega t \\ \alpha_d(t) &= A_{31} + A_{32}\sin\omega t + A_{33}\cos\omega t + A_{34}\sin 0.5\omega t\end{aligned} \tag{1}$$

At the beginning of each run, each DOF is driven from its zero angle to the initial desired trajectory angle using a quintic polynomial trajectory over the period of 1 second. A quintic polynomial ensures a smooth transition into the desired trajectory by matching the angle, angular velocity, and angular acceleration at the transition point[9]. Similarly, each DOF is driven from its final desired trajectory angle to its zero angle at the end of each run using a quintic polynomial trajectory. Following the initial transition from rest, the wing is driven for 6 periods at the frequency ω = 3.14 rad/s, or 12 seconds. This is followed by a 1 second transition back to rest. The two transition periods are excluded in evaluating the average vertical force.

G. Computational Optimization

In this section, a coupled virtual *and* physical optimization-based approach for identifying desirable flapping patterns is presented. Specifically, the motivation for coupling the experimental hardware to a computation-based optimizer and the associated challenges are discussed. This is followed by the overarching optimization strategy used in this study and the components thereof, which include a Box-Behnken[10] sampling approach, ridge regression, and two gradient-based optimization formulations.

Computational optimization is used to efficiently search for flapping patterns with desirable characteristics. Efficiency in finding desirable flapping patterns is of particular interest for this study because of the challenges associated with this coupled virtual and physical approach. Challenges include: lengthy function evaluation time (on the order of 30 seconds per evaluation), noisy objective functions, objective function drift over time, and protecting hardware from optimization runs that exceed the limits of the physical hardware.

The overarching optimization strategy is designed to handle these challenges and is based on the tenets that (i) desirable flapping patterns are here taken to be those that result in maximum mean vertical forces as evaluated over the complete path of the flapping pattern; (ii) the search for desirable flapping patterns is efficient when driven by established computational optimization approaches; and (iii) aspects of flapping wing flight aerodynamics are more effectively characterized through instrumented experimentation as opposed to predictive physics-based models (e.g., CFD simulations). Therefore, based on these tenets, the optimization strategy used in this study:

- Maximizes the mean vertical force as evaluated over the complete path of the flapping pattern,
- Uses sequential quadratic programming (SQP) to search for desirable flapping patterns, and
- Uses optimization-determined virtual flapping patterns as target trajectories for the instrumented physical hardware that measures and returns vertical force data to the SQP search algorithm.

The optimization problem statement can be formally written as follows.

$$\min_{A_{11},A_{12},A_{13},A_{14},A_{21},A_{22},A_{23},A_{24},A_{31},A_{32},A_{33},A_{34}} -\overline{F}_z \tag{2}$$

subject to

$$\theta_{i,\max} \le \theta_i^u \quad \forall i \in \{1,2,3\} \tag{3}$$

$$\theta_{i,\min} \ge \theta_i^l \quad \forall i \in \{1,2,3\} \tag{4}$$

$$A_{i,j}^l \le A_{i,j} \le A_{i,j}^u \quad \forall i \in \{1,2,3\}, \forall j \in \{1,2,3,4\} \tag{5}$$

where

$$\theta_{i,\max} = \max\{\theta_i = A_{i,1} + A_{i,2}\sin\omega t + A_{i,3}\cos\omega t + A_{i,4}\sin 0.5\omega t\} \quad \text{for} \quad t = 0 \to t_s \quad \text{and} \quad \forall i \in \{1,2,3\} \tag{6}$$

$$\theta_{i,\min} = \min\{\theta_i = A_{i,1} + A_{i,2}\sin\omega t + A_{i,3}\cos\omega t + A_{i,4}\sin 0.5\omega t\} \quad \text{for} \quad t = 0 \to t_s \quad \text{and} \quad \forall i \in \{1,2,3\} \tag{7}$$

and where $A_{i,j}$ represent the optimization design variables, $\overline{F}_z$ represents the mean measured vertical force, and θ_i is a desired angle trajectory used to drive the i^{th} degree of freedom. Based on this definition, $\theta_1 = \theta_d$, $\theta_2 = \varphi_d$, and $\theta_3 = \alpha_d$. The constraints provided in Eqs. (3, 4) keep the desired trajectories within the limits of the hardware, and the constraint shown in Eq. (5) limits the SQP algorithm to amplitude values between the prescribed lower and upper limits, denoted by *l* and *u*, respectively. Table 1 shows the parameter values used for this study.

Table 1: Optimization parameters

Parameter	Value
θ_1^l	−180°
θ_1^u	180°
θ_2^l	−45°
θ_2^u	55°
θ_3^l	−60°
θ_3^u	60°
$A_{i,j}^l \quad i = 1, \forall j \in \{1,2,3,4\}$	−90°
$A_{i,j}^l \quad \forall i \in \{2,3\}, \forall j \in \{1,2,3,4\}$	−30°
$A_{i,j}^u \quad i = 1, \forall j \in \{1,2,3,4\}$	−90°
$A_{i,j}^u \quad \forall i \in \{2,3\}, \forall j \in \{1,2,3,4\}$	30°
ω	3.14 rad/s
t_s	14 s

A two-stage approach is used to protect the hardware from being exposed to a driving function that exceeds the hardware's capabilities. Such a strategy is needed when using the SQP approach because SQP can use infeasible solutions to aid the search for optimal solutions. To that end, an artificial infeasible solution is provided to the optimizer when conditions that would damage the hardware are detected. The first stage of protection is found within the optimization constraints. These constraints encourage the search to stay within a safe region. The second stage of protection is implemented directly before a driving function is sent from the optimizer to the hardware. Here, the candidate driving function is evaluated by invoking Eqs. (6, 7). When these values are found to be outside of the prescribed limits, the invoking of the hardware is excluded from the process and an artificial, and not desirable, function value is returned to the optimizer.

Two approaches for handling objective function noise (i.e., noise from the load cell) are used in this study. The first is a strategic sampling of the design space to identify a desirable initial design for the gradient-based optimization algorithm. The second is to use a relatively large minimum step size in the SQP algorithm. Due to the lengthy function evaluation time associated with this experiment, a Box-Behnken sampling approach is used[10]. The Box-Behnken approach requires 204 runs to fit a 12-variable quadratic response surface to the data. The full quadratic response surface is given as

$$\hat{F}_z = \beta_0 + \sum_{i=1}^{n_s} \beta_i x_i + \sum_{i=1}^{n_s} \beta_{ii} x_i^2 + \sum_{i=1}^{n_s-1} \sum_{j=i+1}^{n_s} \beta_{ij} x_i x_j \tag{8}$$

where $\hat{F}_z$ is the predicted mean vertical force, β are the response surface coefficients, n_x is the number of variables, and $[x_1\ x_2\ \ldots\ x_{12}] = [A_{1,1}\ A_{1,2}\ A_{1,3}\ A_{1,4}\ A_{2,1}\ A_{2,2}\ A_{2,3}\ A_{2,4}\ A_{3,1}\ A_{3,2}\ A_{3,3}\ A_{3,4}]$. The following linear regression is used to identify β:

$$\beta = (V^{\mathrm{T}}V + \alpha I)^{-1}V^{\mathrm{T}}R \tag{9}$$

where V is a matrix of data regarding the problem variables, R is a vector of objective function responses, I is the identity matrix, and α is a scalar set to 0.0001.

It is important to note that under the coupled virtual and physical optimization approach presented here, the hardware limits must be considered and strictly observed during the sampling. This requires an additional optimization problem formulation to be used in conjunction with the Box-Behnken sampling strategy. Consider, for example, the first three experiments of the 12-variable Box-Behnken sampling strategy:

$$\begin{bmatrix} -1 & -1 & 0 & 0 & -1 & 0 & -1 & 0 & 0 & 0 & 0 & 0 \\ -1 & -1 & 0 & 0 & -1 & 0 & 1 & 0 & 0 & 0 & 0 & 0 \\ -1 & -1 & 0 & 0 & 1 & 0 & -1 & 0 & 0 & 0 & 0 & 0 \\ & & & & & \vdots & & & & & & \end{bmatrix} \tag{10}$$

For Eq. (10), each column represents one of the 12 variables and the rows represent the experiments to be considered. Each value in the matrix represents a variable's value set to a high, low, or central value. When a particular experiment is identified as one that will violate the limits of the hardware, the experiment cannot be run. To maintain the required number of experiments to fit a quadratic response surface, an alternative experiment must be run. A new experiment, as similar to the proposed experiment as possible, yet within the limits of the hardware, is identified by the following optimization problem statement.

$$\min_{A_{i,j}} \quad \sum_{i=1}^{3}\sum_{j=1}^{4}\left(A_{i,j} - \tilde{A}_{i,j}\right)^2 \tag{11}$$

subject to Eqs. (3-7) and where $\tilde{A}_{i,j}$ represents the experiment proposed by the Box-Behnken approach. This problem statement results in a modified Box-Behnken sampling strategy with modifications as illustrated by Eq. (12) for a first experiment (row 1) that violates the hardware limits.

$$\begin{bmatrix} -0.978 & -0.924 & 0 & 0 & -0.864 & 0 & -0.900 & 0 & 0 & 0 & 0 & 0 \\ -1 & -1 & 0 & 0 & -1 & 0 & 1 & 0 & 0 & 0 & 0 & 0 \\ -1 & -1 & 0 & 0 & 1 & 0 & -1 & 0 & 0 & 0 & 0 & 0 \\ & & & & & \vdots & & & & & & \end{bmatrix} \tag{12}$$

Finally, to reduce the problem of objective function drift, force bias is subtracted at the beginning of each run. In the following section, initial results are presented and discussion is provided regarding future work.

III. Initial Results

A 12-variable Box-Behnken design of experiments was conducted over the complete design space from the lower bounds to the upper bounds. This set of experiments was used to identify a starting design for the gradient-based optimization algorithm. Two strategies were used to solve the optimization problem; one used a minimum variable change of 5 degrees, and the other used a minimum variable change of 10 degrees. It was found that a minimum variable change of 5 degrees was insufficient to lead to meaningful convergence, presumably because of noise in the force signal. The minimum variable change of 10 degrees, however, led to convergence evidenced by a noticeable improvement in mean vertical force generated by the flapping wing.

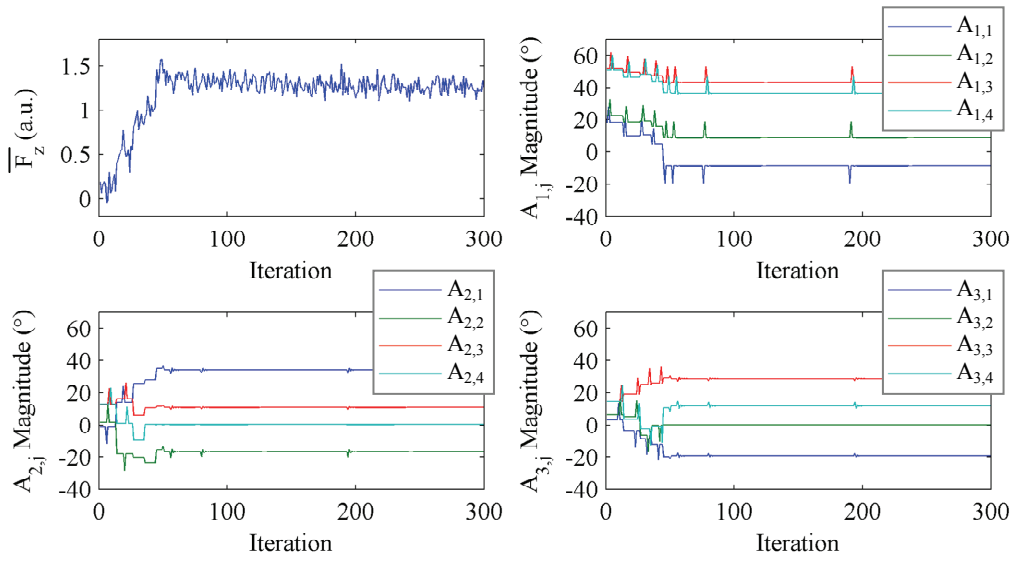

Figure 4. Mean vertical force ($\overline{F}_z$; arbitrary units) convergence plot (top left) and coefficient variable values (top right; bottom row).

Figure 4 shows results from one optimization run using 10 degree minimum variable change and starting design variables [x_1 x_2 ... x_{12}] = [18.2 22.6 51.9 50.4 −1.37 −1.74 12.5 12.8 3.33 6.21 14.4 14.4]. These variables were established by the Box-Behnken design of experiments and trial optimization runs. It can be seen that the initial design variables (corresponding to iteration 0) yielded a $\overline{F}_z$ value near zero. The optimization reached a plateau after approximately 50 iterations. Experimental noise can be seen in the $\overline{F}_z$ signal fluctuations in spite of relatively constant design variables. The design variables after approximately 300 iterations were [x_1 x_2 ... x_{12}] = [−8.89 8.96 43.2 36.5 34.3 −16.9 10.7 0.42 −19.5 0.33 28.7 11.6].

Figure 5 shows the three rotation angles vs. time and the corresponding instantaneous F_z data for iterations 1 and 300. The improvement in F_z vs time, evidenced by a higher $\overline{F}_z$, demonstrates the effectiveness of the optimization strategy.

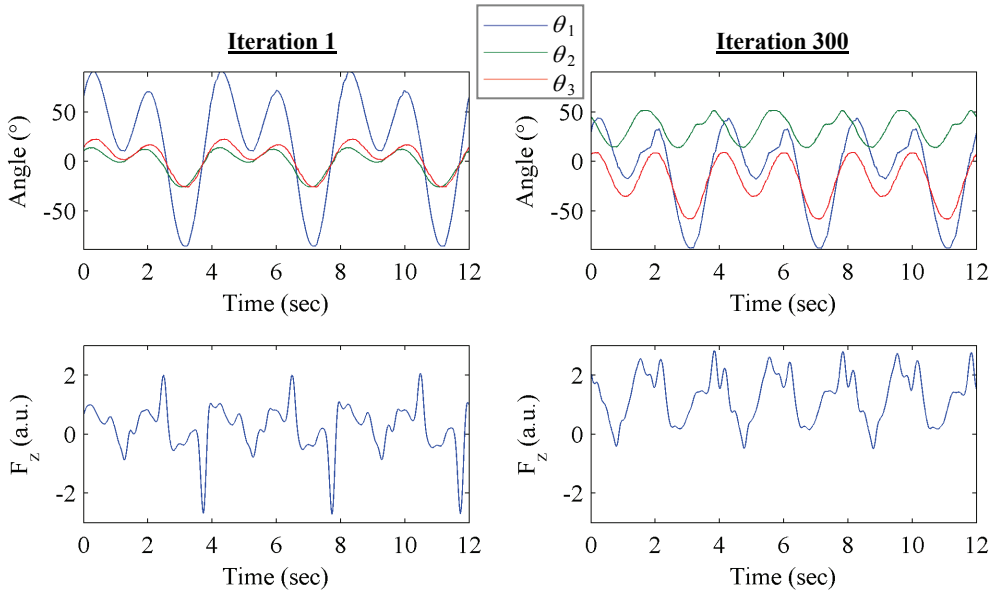

Figure 5. Rotation angles vs. time for iteration 1 (top left) and iteration 300 (top right). Instantaneous vertical force (arbitrary units) vs. time for iteration 1 (bottom left) and iteration 300 (bottom right).

IV. Conclusions, Summary, and Future Work

The work presented here represents initial results on optimizing the trajectory of a flapping wing mechanism. The results illustrate the functionality of the measurement hardware, controller, and optimization methods and software, and demonstrate the feasibility of optimizing complex wing trajectories based on measured vertical force. These initial studies in connecting the virtual and the physical domains have been used to identify challenges and give promise to the approaches used to overcome them. It is hoped that future development will enable contributions towards further understanding the physical foundations of flapping flight, especially with compliant wings, through aerodynamic studies of optimal wing trajectories using coupled experimental-computational optimization methods.

Our current experimental setup allows for control and measurement of one flapping wing with three degrees of freedom. Our immediate plans, and those from which we anticipate further results, include the following:

1) Addition of a second wing to allow more realistic simulation of the aerodynamics of flapping wing flight.
2) Additional optimization objectives, such as efficiency.
3) Inclusion of more Fourier terms in the path definitions to allow for a wider variety of prescribed trajectories.
4) Investigation of the aerodynamics of the optimal paths (e.g., using Particle Image Velocimetry).
5) Modified optimization approaches.

Regarding the last item, two basic optimization approaches and a hybrid of the two are the focus of current work in identifying optimal flapping patterns. They are described briefly here. The first approach uses a response surface methodology coupled with gradient-based optimization to find the most desirable flapping patterns. Under this approach, a series of response surfaces are constructed; the first surfaces are large with poor accuracy, while the final surfaces are small and accurate. A gradient-based algorithm searches the response surface. Statistical sampling near regions of interest is needed and carried out using the Box-Behnken approach. The second strategy is to explore the use of small-population genetic algorithms. This approach becomes more desirable when objective function modality and noise continue to pose challenges that are not overcome by the smoothing effect of the response surface methodology. Finally a hybrid approach may be used to reduce the computational expense of the genetic algorithm by directing populations and generations to desirable regions of the design space as identified through the response surface method, or through the reduced sample statistical studies.

Acknowledgments

The authors thank Kevin Cole, Terrence Hess, Ryan George, and Kenneth P. Clark for their contributions to the project. Support of a research initiation grant from the Brigham Young University Ira A. Fulton College of Engineering and Technology is gratefully acknowledged.

References

[1]McMichael, J. M., and Francis, M. S. "Micro Air Vehicles – Toward a New Dimension in Flight," DARPA, USA, 1997.

[2]Shyy, W., Lian, Y., Tang, J., Viieru, D., and Liu, H. *Aerodynamics of Low Reynolds Number Flyers*, Cambridge University Press, Cambridge, 2008, Chaps. 1, 4.

[3]Dickinson, M. H., Lehmann, F.-O., and Sane, S. P. "Wing Rotation and the Aerodynamic Basis of Insect Flight," *Science*, Vol. 284, 18 June 1999, pp. 1954-1960.

[4]Conn, A. T., Burgess, S. C., and Ling, C. S. "Design of a parallel crank-rocker flapping mechanism for insect-inspired micro air vehicles," *Proceedings of the I MECH E Part C Journal of Mechanical Engineering Science*, Vol. 221, No. 10, 2007, pp. 1211-1222.

[5]Bandyopadhyay, P. R., Beal, D. N., and Menozzi, A. (2008). "Biorobotic insights into how animals swim," *The Journal of Experimental Biology*, Vol. 211, 2008, pp. 206-214.

[6]Liu, H., Ellington, C. P., Kawachi, K., van den Berg, C., and Willmott, A. P. "A Computational Fluid Dynamic Study of Hawkmoth Hovering," *The Journal of Experimental Biology*, Vol. 201, 1998, pp. 461-477.

[7]Van den Berg, C., and Ellington, C. P. "The Vortex Wake of a 'Hovering' Model Hawkmoth," *Philosophical Transactions of the Royal Society B: Biological Sciences*, Vol. 352, No. 1351, 29 Mar. 1997, pp. 317-328.

[8]Aono, H., Liang, F., and Liu, H. "Near- and far-field aerodynamics in insect hovering flight: an integrated computational study," *The Journal of Experimental Biology*, Vol. 211, 2008, pp. 239-257.

[9]Spong, M.W., Hutchinson, S., and Vidyasagar, M. *Robot Modeling and Control*, Wiley & Sons, 2006, Chap. 5.

[10]Box, G. E. P., and Draper, N. R. *Empirical Model Building and Response Surfaces*, John Wiley and Sons, New York, 1987, p. 477.